Fermionization dynamics of a strongly interacting one-dimensional Bose gas after an interaction quench

2010 New J. Phys. 12 083065

(http://iopscience.iop.org/1367-2630/12/8/083065)

New Journal of Physics
The open-access journal for physics

Fermionization dynamics of a strongly interacting one-dimensional Bose gas after an interaction quench

Dominik Muth[1,3], **Bernd Schmidt**[1,2] **and Michael Fleischhauer**[1]

[1] Fachbereich Physik und Forschungszentrum OPTIMAS, Technische Universität Kaiserslautern, D-67663 Kaiserslautern, Germany
[2] Institut für Theoretische Physik, Johann Wolfgang Goethe-Universität, D-60438 Frankfurt am Main, Germany
E-mail: muth@physik.uni-kl.de

New Journal of Physics **12** (2010) 083065 (11pp)
Received 11 May 2010
Published 31 August 2010
Online at http://www.njp.org/
doi:10.1088/1367-2630/12/8/083065

Abstract. We study the dynamics of a one-dimensional Bose gas after a sudden change of the interaction strength from zero to a finite value using the numerical time-evolving block decimation (TEBD) algorithm. It is shown that despite the integrability of the system, local quantities such as the two-particle correlation $g^{(2)}(x, x)$ attain steady-state values in a short characteristic time inversely proportional to the Tonks parameter γ and the square of the density. The asymptotic values are very close to those of a finite temperature grand canonical ensemble, with a local temperature corresponding to the initial energy and density. Non-local density–density correlations, however, approach a steady state on a much larger time scale determined by the finite propagation velocity of oscillatory correlation waves.

[3] Author to whom any correspondence should be addressed.

Contents

1. Introduction

The dynamics of interacting quantum systems from an initial non-equilibrium state constitutes a major challenge for many-body theory. In particular, the question of the thermalization of integrable models regained attention recently due to the experimental progress in ultracold gases. As demonstrated in a beautiful experiment by Kinoshita *et al* [1] for the example of a one-dimensional (1D) ultracold Bose gas, integrable systems do not thermalize in the usual sense, i.e. reduced density-matrices relax on considerably different time scales than in the absence of integrability.

The peculiarity of the relaxation dynamics of integrable systems has been attributed to the presence of an infinite set of constants of motion with local character, i.e. which can be written as sums of operators acting only over a finite spatial range. Although thermalization has been studied in a large body of theoretical papers, it remains a largely unsolved problem. Most studies of specific models have been done either for non-interacting particles [2] or for systems that can be mapped directly to free systems such as hard-core bosons [3], the Luttinger model [4] or the $1/r$ fermionic Hubbard model [5].

In the present paper, we analyse the dynamics of a 1D Bose gas with s-wave scattering interactions, described by the Lieb–Liniger (LL) model, after a sudden quench of the interaction strength from zero to a finite value, covering the full range from weak to strong interactions. Performing numerical simulations using the time-evolving block decimation algorithm (TEBD) [6, 7], we show that local quantities, in particular the local two-particle correlation $g^{(2)}(0, 0; t)$, do approach steady-state values on a short time scale determined only by the Tonks parameter γ and the particle density ϱ. This shows that although non-local quantities such as the momentum distribution do not approach a steady state over long times [8], there is an equilibration in a local sense. Furthermore, the asymptotic values of $g^{(2)}(x, x)$ are very close to those obtained from a thermal Gibbs ensemble [9], with temperature and chemical potential determined by the initial conditions and the amplitude of the interaction quench. Thus, it is possible to define local temperature and chemical potential, and the influence of constants of motion other than total energy and particle number is very small, if present at all. Non-local quantities such as the density–density correlation approach a steady-state distribution on a larger time scale by way of correlation waves propagating out of the sample.

2. The Lieb–Liniger (LL) model and lattice approximation

A Bose gas in one spatial dimension is described by the Hamiltonian

$$\hat{H} = \int \mathrm{d}x \left[\hat{\Psi}^\dagger(x) \left(-\frac{1}{2}\partial_x^2 \right) \hat{\Psi}(x) + \frac{g}{2}\, \hat{\Psi}^{\dagger\,2}(x)\hat{\Psi}^2(x) + \hat{\Psi}^\dagger(x) V(x) \hat{\Psi}(x) \right] \tag{1}$$

in units where $\hbar = m = k_\mathrm{B} = 1$. Here, $\hat{\Psi}(x)$ is the field operator of the Bose gas in second quantization, $V(x)$ some possible trap potential and g the strength of the local particle–particle interaction. The latter is characterized by the dimensionless Tonks parameter $\gamma = g/\varrho$, where $\varrho = \langle \hat{\Psi}^\dagger(x)\hat{\Psi}(x) \rangle$ is the 1D density of particles. Specifically, we consider here a system initially prepared in the non-interacting ground state.

The initial *canonical* state has locally only diagonal elements. In the course of interactions, non-diagonal elements are not created. Thus, the reduced local density matrix is entirely determined by the number distribution, and the quantities of interest are the density ρ and the local two-particle correlation $g^{(2)}(x, x, t)$, where

$$g^{(2)}(x, y, t) = \frac{\langle \hat{\Psi}^\dagger(x)\hat{\Psi}^\dagger(y)\hat{\Psi}(y)\hat{\Psi}(x) \rangle}{\varrho(x)\varrho(y)}. \tag{2}$$

In principle, the corresponding higher-order moments are also non-zero. They will, however, not be considered here.

We study the dynamics after the interaction quench numerically by means of the TEBD algorithm [6, 7]. As for any numerical methods, this requires the use of a discretized version of the LL model. The discretization of the LL model leads to the (non-integrable) Bose–Hubbard model [10]

$$\hat{H} = -J \sum_j (\hat{a}_j^\dagger \hat{a}_{j+1} + \text{h.a.}) + \frac{U}{2} \sum_j \hat{a}_j^{\dagger\,2} \hat{a}_j^2 + D \sum_j \hat{a}_j^\dagger \hat{a}_j, \quad x_j = j\,\Delta x. \tag{3}$$

Here, $J = 1/(2\Delta x^2)$, $U = g/\Delta x$ and $D = 1/\Delta x^2$, with Δx being the lattice constant of the discretization grid. The appropriateness of discretized lattice models for describing continuous interacting Bose or Fermi gases in the limit $\Delta x \to 0$ has been discussed and verified in a number of earlier papers [10, 11]. Note, furthermore, that using the boson–fermion duality in 1D, the LL model can be mapped to an integrable lattice model, the spin-1/2 *XXZ* model [11]. For some data sets we used both equation (3) and the XXZ lattice model to verify that in the considered limit the non-integrability of (3) has no influence on the results.

It emerged that for the simulation of dynamics the necessary grid sizes are much smaller than for equilibrium simulations [10, 11]. Empirically, we found that in order to minimize lattice artefacts resulting in numerical errors, the average number of particles per lattice site $\langle \hat{n} \rangle$ should be small compared to $1/\gamma$, where $\gamma = g/\varrho$ corresponds to the density at the centre of the cloud, i.e. $\varrho \to \varrho(x = 0)$. This can be explained as follows. The interaction energy of a two-particle collision in the lattice, i.e. $g/\Delta x$, should be smaller than the bandwidth of the lowest Bloch band, $\sim 1/\Delta x^2$, in order not to see lattice artefacts. At the edges of the cloud where collisions become less probable the condition is less strong. To accommodate the requirement of a very small $\langle \hat{n} \rangle$ at the centre of the cloud, we used space-dependent grid sizes such that the average boson number per site was constant for the central part of the particle distribution. Nevertheless, to approximate the continuous model sufficiently well, very fine grids were needed, leading to

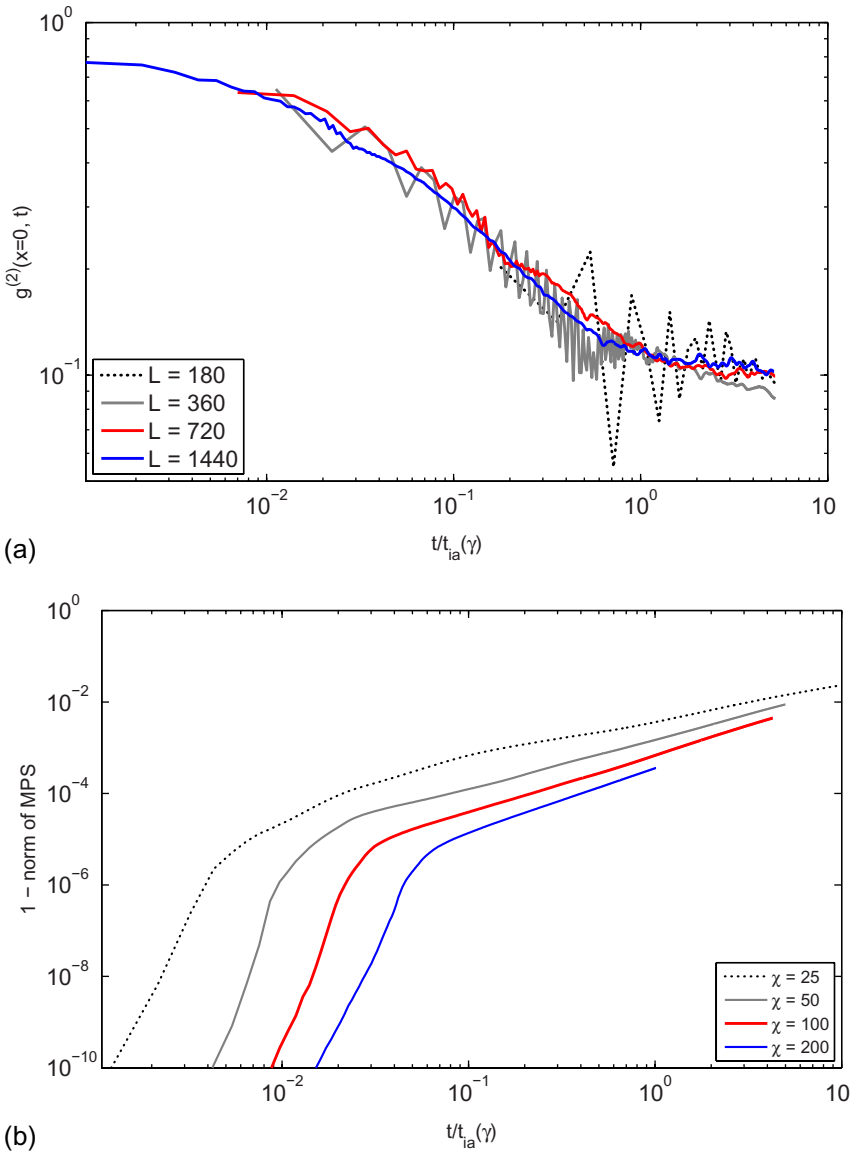

Figure 1. (a) Time evolution of normalized local two-particle correlation $g^{(2)}(0, 0; t)$ (see section 3) for $N = 9$ particles and $\gamma = 200/9$ for increasing lattice length, corresponding to finer grid sizes. One clearly recognizes oscillations that are lattice artefacts and that only disappear for the largest lattice sizes. (b) Accumulated truncation error of the norm of the MPS in the dynamical TEBD algorithm for $\gamma = 200/9$ and increasing bond dimension χ.

quite large lattice sizes of the order of up to 2880, which is challenging. In order to illustrate the effects of discretization we have plotted in figure 1(a) the local two-particle correlation (see the following section) for $\gamma = 200/9$ and increasing lattice sizes L, corresponding to finer grids. One clearly recognizes oscillation artefacts, which only slowly disappear with increasing L.

The convergence of the TEBD scheme was checked by varying the bond dimension χ of the matrix product state (MPS) and calculating the truncation error in the state norm accumulated during the time evolution. In figure 1(b) the accumulated truncation error is plotted

for $\gamma = 200/9$ and increasing values of χ from 25 to 200. One recognizes that for the maximum value of $\chi = 200$ that we were able to use, the truncation error is below the level of 10^{-3} for the time scale of interest. This value is larger than the accuracy typically reached in ground state calculations. However, we are not at the point where the cut-off explodes, which typically happens in dynamical simulations at some point. Finally, the matrix dimension required to achieve a given accuracy does not depend on the discretization length, i.e. the number of lattice sites used. It is rather the number of particles that determines the complexity of the calculations. Thus the restriction to a moderate particle number allows us to work on a lattice large compared to other applications of the algorithm.

3. Local dynamics

In order to be able to perform numerical simulations with a fixed number of particles (up to 18, which corresponds to the experiments in [12, 13]), we have to work with a finite size system. Therefore, we assumed an initial weak harmonic trapping potential $V(x) = \frac{1}{2}\omega^2 x^2$. Open or periodic boundary conditions, which can also be dealt with by the TEBD algorithm, could be used alternatively. Initially, the Bose gas is in the canonical ground state ($T = 0$) of non-interacting bosons in the trap, for which the matrix product representation is analytically known, since it is a product of single-particle states. At $t = 0$, we suddenly switch the interaction strength from zero to a finite value. At the same time, the trap, whose only purpose was the preparation of an appropriate initial state, is switched off. On the time scales we are interested in, the density distribution does not change, so that the presence of a trap would be of no relevance. This also allows us to apply the results of the present analysis to a homogeneous gas.

The initial state has a Gaussian density distribution $\varrho(x) = N\sqrt{\frac{\omega}{\pi}}\,\mathrm{e}^{-\omega x^2}$ with $l_{\mathrm{osc}} = \frac{1}{\sqrt{\omega}}$ being the oscillator length. Figure 2 shows the time evolution of $g^{(2)}(0, 0; t)$ with time normalized to a characteristic time scale t_{ia} for different values of γ. One recognizes after an initial phase a power-law decay with an exponent that is monotonic in the interaction parameter. At times close to t_{ia}, a steady-state value is attained, indicating that a local equilibrium is reached. That is, although globally an LL gas does not thermalize [1], local quantities do. The time scale t_{ia} of the local dynamics can be estimated from equation (3). The repulsive interaction $U\hat{n}(\hat{n} - 1)$ causes particle number fluctuations to be driven out of a given lattice site. This happens in the following way. Initially, all components of the state vector have the same phase and tunnelling has no effect. However, due to the interaction, components with different particle numbers attain a differential phase shift and are subsequently coupled to states in adjacent lattice sites by tunnelling with rate J. Since in the limit $\Delta x \to 0$ we have $J \gg U$, the maximum rate of this process is limited by the average interaction energy per particle $U\langle\hat{n}\rangle$. Thus, we have

$$t_{\mathrm{ia}} = \frac{1}{U\langle\hat{n}\rangle} = \frac{1}{g\varrho} = \frac{1}{\gamma\varrho^2}. \tag{4}$$

Note that already for moderate interaction strength, $\gamma \gg 1/N^2$, this time is much shorter than, for example, the oscillation time t_{osc} in the trap.

$$t_{\mathrm{ia}} \sim \frac{l_{\mathrm{osc}}^2}{\gamma N^2} = t_{\mathrm{osc}}\frac{1}{\gamma N^2} \ll t_{\mathrm{osc}}. \tag{5}$$

Note, furthermore, that although the characteristic time of the expansion of the gas after switching off the trap becomes much shorter than t_{osc} for larger interactions, we found that

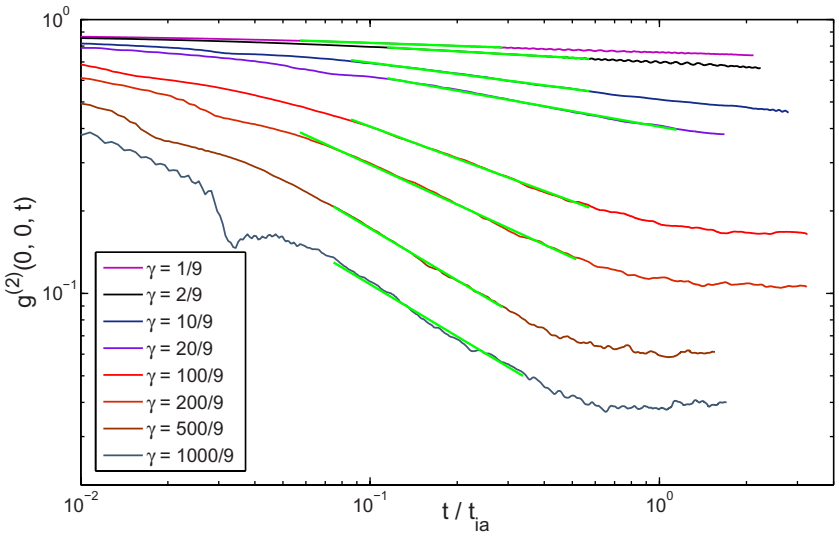

Figure 2. Time evolution of normalized local two-particle correlation $g^{(2)}(0, 0; t)$ after a sudden switch on of interactions at $t = 0$ obtained from a numerical TEBD simulation for nine particles initially prepared in the non-interacting ground state of a harmonic trap. An intermediate power-law decay with an exponent that is monotonic in γ is apparent. The lattice size was up to $L = 2880$ for the strongest interactions corresponding to a lattice spacing of $\Delta x / l_{\mathrm{osc}} \approx 6.15 \times 10^{-4}$ at the trap centre.

the density profile did not change on the scale of t_{ia} even for the largest values of γ used, since also $t_{\mathrm{ia}} \sim 1/\gamma$. Note, furthermore, that although the characteristic time of the expansion of the gas after switching off the trap becomes much shorter than t_{osc} for larger interactions, it will be large compared to t_{ia}. This is because the kinetic energy transferred to the particles will be of the order γ and therefore their characteristic speed will be of the order $\sqrt{\gamma}$ only. Accordingly, we found numerically that the density profile did not change on the time scale t_{ia}, even for the largest values of γ used. Whether or not the thermalized local correlation will adiabatically follow the density evolution after longer times, i.e. when the expansion of the cloud sets in, cannot be concluded from our simulations. We would, however, expect such a behaviour.

The fluctuations in the plots are artefacts of the discretization, which leads to an oscillatory behaviour of $g^{(2)}$ on top of the continuous-system time evolution. These artefacts, which are most pronounced for larger interactions, could not be eliminated completely, even for the smallest grid sizes used. As a result, the asymptotic values of $g^{(2)}(0, 0, t)$ can only be given with a certain error.

In figure 3, we have plotted the exponents obtained from a fit to the curves in figure 2, which for intermediate times follows a power law

$$g^{(2)}(0, 0; t) \sim \left(\frac{t}{t_{\mathrm{int}}}\right)^{\alpha - 1}. \tag{6}$$

The exponent is a monotonic function of the interaction strength and slowly approaches the limit -1 for $\gamma \to \infty$, i.e. for a Tonks–Girardeau gas [14].

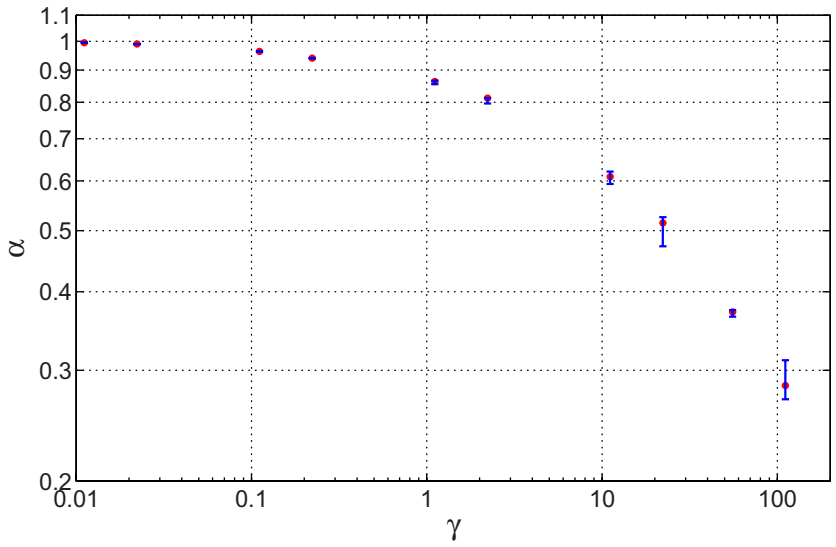

Figure 3. Exponents $\alpha - 1$ of the intermediate power-law decay of $g^2(0, 0; t)$ in figure 2 as a function of γ. Error bars indicate systematic fitting errors.

We now want to analyse the local state of the system in the stationary limit. In particular, we will show that the local steady state can be well described by the usual finite-temperature Gibbs state. To this end, we calculate the expected asymptotic value $g^{(2)}_{YY}(0, 0)$ from the thermodynamic Bethe Ansatz [9]. The system is initially prepared in its non-interacting ground state, so we have $g^{(2)}_{\mathrm{ini}}(0, 0) = 1 - 1/N$, which in the thermodynamic limit $N \to \infty$ approaches unity. The energy of this state with respect to the non-interacting Hamiltonian is 0. At time $t = 0$, the interaction is switched to a finite strength $g > 0$ and the expectation value of the interaction energy immediately after the quench is given by

$$E_{\mathrm{ia}} = \int \mathrm{d}x \, \frac{g}{2} \langle \hat{\Psi}^{\dagger\,2}(x) \hat{\Psi}^2(x) \rangle = \int \mathrm{d}x \, \frac{\gamma}{2} g^{(2)}(x, x) \varrho^3(x). \tag{7}$$

Since in a homogeneous system there is no x-dependence, the energy per particle is

$$\left. \frac{E}{N} \right|_{t=0+} = \left. \frac{E_{\mathrm{ia}}}{N} \right|_{t=0+} = \gamma T_{\mathrm{c}}. \tag{8}$$

Here, we have introduced the critical temperature T_{c} in one dimension $T_{\mathrm{c}} = \varrho^2/2$. One recognizes that the system is in a highly excited non-equilibrium state after the quench if $\gamma \gtrsim 1$. Using the energy per particle, the density ϱ and the Tonks parameter γ as input parameters, we can extract a temperature T of a corresponding thermal Gibbs state by inverting the Yang–Yang equations of the thermodynamic Bethe ansatz [9] for the excitation energy and particle densities $\epsilon(q)$ and $n(q)$ in momentum space:

$$\epsilon(\lambda) = \frac{\lambda^2}{2} - \mu - \frac{T}{2\pi} \int_{-\infty}^{\infty} \mathrm{d}\xi \, K(\lambda, \xi) \ln\left(1 + \mathrm{e}^{-\epsilon(\xi)/T}\right),$$

$$2\pi \, n(\lambda) \left(1 + \mathrm{e}^{\epsilon(\lambda)/T}\right) = 1 + \int_{-\infty}^{\infty} \mathrm{d}\xi \, K(\lambda, \xi) \, n(\xi).$$

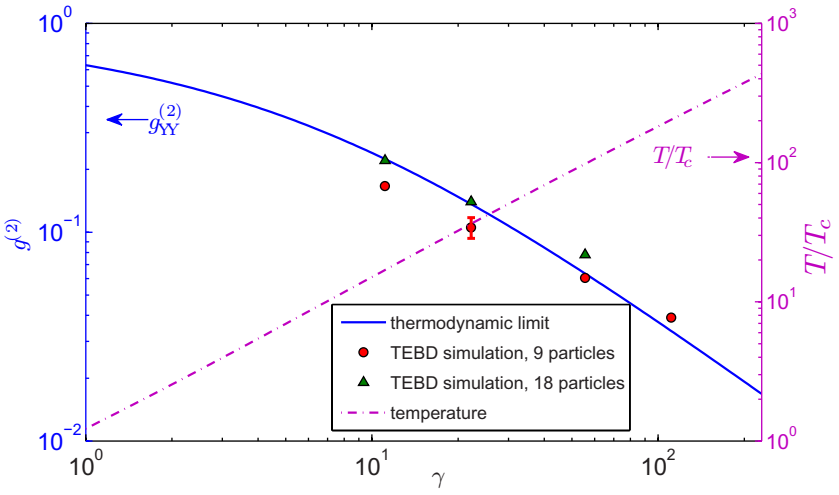

Figure 4. Steady-state values of $g^{(2)}(0,0)$ (left scale) for different values of the interaction parameter γ after the interaction quench obtained from TEBD simulations using nine (red circles, corresponding to figure 2) and 18 (green triangles) bosons. Solid line: value from thermal Gibbs state in the thermodynamic limit; dot dashed line: temperature (right scale) corresponding to the given energy per particle in the thermodynamic limit. The error bar reflects discretization error estimated by comparing steady-state values for $L = 720$ and $L = 1440$ lattice sites, as well as the error resulting from finite MPS matrix dimensions obtained from comparing results for bond dimensions $\chi = 100$ and 200.

Here, $K(\lambda, \xi) = \frac{2g}{g^2+(\lambda-\xi)^2}$ and $\varrho = \int \mathrm{d}\lambda\, n(\lambda)$. With the help of the Hellmann–Feynman theorem, we can then obtain the value $g^{(2)}_{YY}(0,0)$ corresponding to the Gibbs state at temperature T [15]:

$$g^{(2)}_{YY}(0,0) = \frac{2}{\varrho^2}\frac{\partial}{\partial\gamma} f(\gamma, T), \tag{9}$$

with $f(\gamma, T)$ being the free energy per particle,

$$f(\gamma, T) = \mu - \frac{T}{2\pi\rho}\int_{-\infty}^{\infty} \mathrm{d}\xi\ \ln\left(1 + \mathrm{e}^{-\epsilon(\xi)/T}\right). \tag{10}$$

In the limit $1 \ll \tau \ll \gamma^2$, where $\tau = T/T_c$, equation (9) attains the simple form [15]

$$g^{(2)}_{YY}(0,0) = \frac{2\tau}{\gamma^2}. \tag{11}$$

In figure 4, we have plotted the values of $g^{(2)}_{YY}(0,0)$ from the thermal Gibbs state in the thermodynamic limit as a function of the interaction strength γ (solid line). Also shown are the steady-state values obtained from the numerical simulation in figure 2. The error bar indicates uncertainties, which are here due to discretization artefacts and error estimates obtained from comparing simulations with MPS bond dimensions $\chi = 100$ and 200. It is available only for one parameter set, since the variation of the discretization length and the bond dimension is numerically expensive. However, we expect it to be of about the same relative size for all data points. One recognizes that $g^{(2)}(0,0;t)$ attains values in the long-time limit that are close to

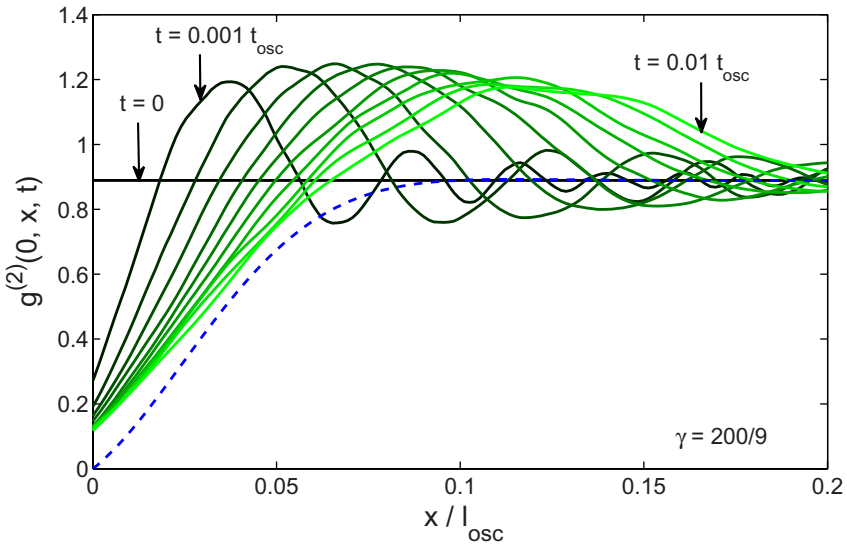

Figure 5. Time evolution of non-local density–density correlations $g^{(2)}(0, x; t)$ for $\gamma = 200/9$. Here, $x = 0$ denotes the centre of the cloud. One recognizes the formation of expanding correlation waves. The dashed blue line shows the approximation (13) to the non-local correlation in a thermal Gibbs state from [16] multiplied by $g^{(2)}(0, 0, t = 0) = 8/9$ to account for the final particle number ($N = 9$) used in the simulation.

those of the thermal Gibbs state. One should note that the steady-state values for the largest values of γ ($\gamma = 500/9$ and 18 bosons, as well as $\gamma = 1000/9$ and 9 bosons) are slightly overestimated in the simulation due to the remaining grid artefacts, since here $\langle\hat{n}\rangle\gamma \approx 0.73$ is no longer small compared to unity. Also shown is the asymptotic local temperature of the gas in units of the degeneracy temperature. For large values of γ, $T \gg T_c$, i.e. after relaxation the gas is in a state with large local temperature.

4. Non-local relaxation

We now discuss the dynamics of non-local quantities. Specifically, we consider the non-local two-particle correlation $g^{(2)}(0, x; t)$. In figure 5, we have plotted $g^{(2)}(0, x; t)$ for different times after the interaction quench. One recognizes that while the local correlations attain a steady-state value on a short time scale, the non-local evolution happens much more slowly. Switching on the particle–particle repulsion leads to a fast reduction of the probability to find two particles at the same position. Associated with this is a correlation flow to larger distances leading to expanding correlation waves. For very short times, the propagation velocity of correlation waves is faster than the Fermi velocity $v_F = \pi\varrho$. But at the largest time shown in figure 5 corresponding to $t = 0.01t_{osc}$, the maximum of the correlation wave has travelled a distance of approximately $\Delta x = 0.12l_{osc}$, which is consistent with the speed of sound, which for large values of γ approaches

$$v_s = v_F\left(1 - \frac{4}{\gamma}\right). \tag{12}$$

The buildup of a maximum that behaves like a wavefront can be understood as follows. The integral over space of $g^{(2)}(0, x; t)$ is (in a homogeneous system) a constant with respect to time due to particle number conservation. The numerator of $g^{(2)}(0, x; t)$ is proportional to the joint probability distribution of finding a particle at position x given that there is one particle at the origin.

So as the quench cannot change $g^{(2)}(0, x; t)$ significantly outside the light cone given by the Fermi velocity, the reduction in the probability of finding two particles close together must be accompanied by an increase at finite distance.

As one can see from figure 5, the non-local correlation function also approaches, at least for smaller distances in the long-time limit, that of the thermal Gibbs state with temperature and density given by the initial conditions and the Tonks parameter γ. For comparison, we have plotted an approximation to the finite-temperature non-local $g^{(2)}$ from [16], which holds in the regime $1 \ll \tau \ll \gamma^2$:

$$g_{\mathrm{T}}^{(2)}(0, x) = 1 - \left[1 - 4\sqrt{\frac{\pi\tau}{\gamma^2}}\left(\frac{x}{\lambda_{\mathrm{T}}}\right)\right] \mathrm{e}^{-2\pi(x/\lambda_{\mathrm{T}})^2}. \tag{13}$$

Here, $\lambda_{\mathrm{T}} = \sqrt{4\pi/\tau\varrho^2}$ is the thermal de Broglie length.

5. Experimental observation

In the following, we discuss the possibility of testing the local relaxation in an experiment. For this, we make use of the fact that by energy conservation the interaction energy lost by the decrease of $g^{(2)}(0, 0)$ must be gained as kinetic energy, $E_{\mathrm{kin}}(t) = E_{\mathrm{ia}}(t = 0) - E_{\mathrm{ia}}(t)$, and the kinetic energy therefore directly gives the value of $g^{(2)}(0, 0, t)$ in the homogeneous case:

$$E_{\mathrm{kin}}(t) = \int \mathrm{d}x\, \frac{g}{2}\left(1 - g^{(2)}(0, 0; t)\right)\varrho^2. \tag{14}$$

If the interaction is turned on at $t = 0$ and turned off abruptly at some time $t = t_1$, the kinetic energy is the only one remaining in the system and can be used to measure $g^{(2)}(0, 0; t_1)$.

$$g^{(2)}(0, 0; t_1) = 1 - \frac{2}{\gamma\varrho^2}\frac{E_{\mathrm{kin}}^{\mathrm{final}}}{N}. \tag{15}$$

In the experimental setup, the gas must be confined, e.g. by a harmonic trapping potential. So the initial non-interacting state has a Gaussian density distribution. It is also a good assumption that the correlations decay locally, as in the homogeneous system, corresponding to the local density provided the density $\varrho(x)$ remains constant over the time scale of interest. This is indeed the case if $t_{\mathrm{int}} = 1/(\gamma\rho^2) \ll l_{\mathrm{osc}}/v_{\mathrm{s}} \sim l_{\mathrm{osc}}/\rho$. This means that the Tonks parameter must be large compared to $\frac{1}{N}$, which is of course the case we are interested in. We note that the region in the wings of the density distribution which does not fulfil this constraint gives a negligible contribution to the total interaction energy. Of course, measuring the kinetic energy in the trap gives only an average of $\frac{g^{(2)}(x,x)}{\varrho^2(x)}$ over the trap.

6. Summary

Using the TEBD scheme, we have numerically analysed the dynamics of a 1D Bose gas (LL model) after an interaction quench from zero to a finite value. Although globally the 1D Bose

gas does not thermalize, we have shown that local quantities attain a steady-state value on a time scale $t_{\mathrm{ia}} = (\gamma \varrho^2)^{-1}$. Within the achievable accuracy these values are consistent with the assumption that local quantities relax to a thermal Gibbs state, with local temperature determined by the initial energy and chemical potential. Non-local quantities such as the density–density correlation relax on a much longer time scale set by the velocity of sound by means of correlation waves propagating out of the sample.

Acknowledgment

This work was in part supported by SFB TR49 of the Deutsche Forschungsgemeinschaft and the graduate school of excellence MAINZ/MATCOR.

References

[1] Kinoshita T, Wenger T and Weiss D S 2006 A quantum Newton's cradle *Nature* **440** 900–3
[2] Cramer M, Dawson C M, Eisert J and Osborne T J 2008 Exact relaxation in a class of nonequilibrium quantum lattice systems *Phys. Rev. Lett.* **100** 030602
[3] Rigol M, Dunjko V, Yurovsky V and Olshanii M 2007 Relaxation in a completely integrable many-body quantum system: an *ab initio* study of the dynamics of the highly excited states of 1D lattice hard-core bosons *Phys. Rev. Lett.* **98** 050405
[4] Luttinger J M 1963 An exactly soluble model of a many-fermion system *J. Math. Phys.* **4** 1154–62
[5] Kollar M and Eckstein M 2008 Relaxation of a one-dimensional Mott insulator after an interaction quench *Phys. Rev.* A **78** 013626
[6] Vidal G 2003 Efficient classical simulation of slightly entangled quantum computations *Phys. Rev. Lett.* **91** 147902
[7] Vidal G 2004 Efficient simulation of one-dimensional quantum many-body systems *Phys. Rev. Lett.* **93** 040502
[8] Mazets I E and Schmiedmayer J 2009 Restoring integrability in one-dimensional quantum gases by two-particle correlations *Phys. Rev.* A **79** 061603
[9] Yang C N and Yang C P 1969 Thermodynamics of a one-dimensional system of bosons with repulsive delta-function interaction *J. Math. Phys.* **10** 1115
[10] Schmidt B and Fleischhauer M 2007 Exact numerical simulations of a one-dimensional trapped Bose gas *Phys. Rev.* A **75** 021601
[11] Dominik Muth, Michael Fleischhauer and Bernd Schmidt 2010 Discretized versus continuous models of p-wave interacting fermions in one dimension *Phys. Rev.* A **82** 013602
[12] Paredes B, Widera A, Murg V, Mandel O, Fölling S, Cirac I, Shlyapnikov G V, Hänsch T W and Bloch I 2004 Tonks–Girardeau gas of ultracold atoms in an optical lattice *Nature* **429** 277–81
[13] Haller E, Gustavsson M, Mark M J, Danzl J G, Hart R, Pupillo G and Nägerl H C 2009 Realization of an excited, strongly correlated quantum gas phase *Science* **325** 1224–7
[14] Chang D E, Gritsev V, Morigi G, Vuletic V, Lukin M D and Demler E A 2008 Crystallization of strongly interacting photons in a nonlinear optical fibre *Nat. Phys.* **4** 884–9
[15] Kheruntsyan K V, Gangardt D M, Drummond P D and Shlyapnikov G V 2003 Pair correlations in a finite-temperature 1D Bose gas *Phys. Rev. Lett.* **91** 040403
[16] Deuar P, Sykes A G, Gangardt D M, Davis M J, Drummond P D and Kheruntsyan K V 2009 Nonlocal pair correlations in the one-dimensional Bose gas at finite temperature *Phys. Rev.* A **79** 043619